2010-3935

16th AIAA/CEAS Aeroacoustics Conference, 7 - 9 Jun 2010 in Stockholm, Sweden

On the Perfectly Matched Layer for the Boltzmann-BGK Equation and its Application to Computational Aeroacoustics

Elena Craig* and Fang Q. Hu[†]
Old Dominion University, Norfolk, Virginia, 23529, United States

Perfectly Matched Layer (PML) absorbing boundary conditions are proposed for the discreet velocity BGK Boltzmann equation (DVBE). Following a study of the linear waves supported by DVBE, nonreflecting absorbing boundary conditions are derived using a proper space-time transformation, Linear analysis shows that the proposed equations are stable for practical numerical calculations. The accuracy of the absorbing boundary condition is validated by numerical solutions where the Boltzmann-BGK equation is solved by a finite difference scheme. Numerical examples are given to show the effectiveness of the proposed equations. Several IMEX Runge-Kutta schemes are considered to increase efficiency of time integration.

I. Introduction

In recent years, numerical methods based on the Boltzmann-BGK equation have been applied to aeroacoustics simulations. The Boltzmann-BGK equation is based on the gas kinetic theory, which provides a microscopic description of fluid motion.^{1,2} The solution variable is the particle distribution which is a function of the space, time and particle velocity. Compared to the Euler and Navier-Stokes equations, which are the macroscopic governing equations, the Boltzmann-BGK equation has the simplicity of a linear convection equation. In particular, a popular numerical method for directly solving the discretized Boltzmann-BGK equation is the Lattice Boltzmann Method (LBM), which take the full advantages of the linear convection term.³ It is simple to implement, fast in execution, and well suited for parallel computing. Numerical solutions of the Boltzmann-BGK equation by finite difference and finite volume methods have also appeared in literature.⁴⁻⁷

Aeroacoustic problems require accurate nonreflecting boundary conditions in order to simulate open boundaries as the reflections off numerical boundaries can destroy the accuracy of the solution inside the computational domain. Compared to the extensive studies in the traditional Computational Fluid Dynamics, research on the boundary conditions for numerical methods based on the Boltzmann-BGK equations is relatively limited. In Ref. 8, three types of nonreflecting boundary conditions were studied for the discreet velocity Boltzmann equation: the extrapolation method, the C^1 continuity method and an absorbing boundary condition which was formed by adding a damping term to the Boltzmann equation. In Ref. 9, an application of the Perfectly Matched Layer technique to the Lattice Boltzmann Method was studied.

In this paper, we will derive the absorbing boundary condition for the discreet velocity Boltzmann-BGK equation based on the Perfectly Matched Layer (PML) methodology. We start our investigation by an examination of the linear waves supported by the Boltzmann-BGK equation. Our linear wave analysis on a simple 9-velocity discreet Boltzmann-BGK equation shows that it supports the familiar acoustic and vorticity waves, in addition to other highly damped wave modes. The dispersion relations of the acoustic and vorticity waves are found to be similar to those of the Euler equations. Based on the linear wave analysis, it would be possible to construct stable and effective PML equations following the same proper space-time

^{*}Graduate research assistant, Department of Mathematics and Statistics, Norfolk, Virginia

[†]Professor, Department of Mathematics and Statistics, Norfolk, Virginia, AIAA associate fellow

Copyright © 2010 by E. Craig and F. Q. Hu. Published by the American Institute of Aeronautics and Astronautics, Inc. with permission.

transformation used in deriving the PML for the Euler equations.^{10,11} Indeed, as we will show in this paper, the derived PML absorbing equations performs well and are numerically stable in test examples.

The Boltzmann-BGK and the proposed PML equations will be solved numerically by a finite difference method. Due to the stiffness of the collision term, use of explicit time integration schemes would result in an exceedingly small time step. Implicit-Explicit (IMEX) Runge-Kutta schemes will be used in this paper. It is worth pointing out that due to the special form of the BGK collision term, all implicit stages can be treated explicitly. ^{12–14}

The rest of the paper is organized as follows. In sections 2 and 3, the formulation of discreet velocity Boltzmann-BGK equation and its linear wave analysis are given. The derivation of PML absorbing equations are shown in section 4. Numerical methods for the solution of PML equations are discussed in sections 5 and 6, and followed by the numerical results in section 7. Conclusions are given in section 8.

II. The Boltzmann Equation

The continuous Boltzmann equation can be written as

$$\frac{\partial f}{\partial t} + \boldsymbol{\xi} \cdot \nabla_x f + \boldsymbol{a} \cdot \nabla_{\boldsymbol{\xi}} f = \Omega(f) \tag{1}$$

where $\Omega(f)$ represents the collision integral and a is the external force on the particle.

By solving the Boltzmann equation, we are solving for the particle distribution function $f(\boldsymbol{x}, \boldsymbol{\xi}, t)$ in which $\boldsymbol{\xi}$ is the particle velocity vector, \boldsymbol{x} is the spatial position vector, and t is the time. The macroscopic quantities of interest, mass density ρ and momentum density $\rho \boldsymbol{u}$, are obtained from the hydrodynamic moments of the distribution function f. In the Bhatnagar-Gross-Krook (BGK) model of the Boltzmann equation, the collision integral is replaced by an approximation in terms of the Maxwell-Boltzmann distribution function f^{eq} and a relaxation parameter λ .¹⁵ Absent of any external force, the Boltzmann-BGK equation is

$$\frac{\partial f}{\partial t} + \boldsymbol{\xi} \cdot \nabla f = -\frac{1}{\lambda} \left(f - f^{eq} \right) \tag{2}$$

To solve for f numerically, we must first discretize Eq. (2) in velocity space using a finite set of velocity vectors $\{\boldsymbol{\xi}_i\}$. The velocity discretization must satisfy the conservation laws and thus be able to produce accurate macroscopic fluid dynamics.¹⁶ For example, a widely used two dimensional velocity discretization of Eq. (2), referred to as the 2D 9-velocity (D2Q9) model, uses the following discreet velocity set:¹⁷

$$\xi_{1} = c(1,0)^{T} \qquad \xi_{2} = c(0,1)^{T} \qquad \xi_{3} = c(-1,0)^{T} \qquad \xi_{4} = c(0,-1)^{T}
\xi_{5} = c(1,1)^{T} \qquad \xi_{6} = c(-1,1)^{T} \qquad \xi_{7} = c(-1,-1)^{T} \qquad \xi_{8} = c(1,-1)^{T}
\xi_{9} = c(0,0)^{T}$$
(3)

with c is a reference speed.

In this model, the equilibrium distribution is obtained by expanding the Maxwell-Boltzmann distribution function as a second order Taylor series in u^{15}

$$f_i^{eq} = w_i \rho \left[1 + \frac{3 \left(\boldsymbol{\xi}_i \cdot \boldsymbol{u} \right)}{c^2} + \frac{9 \left(\boldsymbol{\xi}_i \cdot \boldsymbol{u} \right)^2}{2c^4} - \frac{3 \left(\boldsymbol{u} \cdot \boldsymbol{u} \right)}{2c^2} \right]$$
(4)

where ρ and u are macroscopic density and velocity respectively and w_i is the weight for velocity ξ_i with

$$w_1 = w_2 = w_3 = w_4 = 1/9$$
 $w_5 = w_6 = w_7 = w_8 = 1/36$ $w_9 = 4/9$ (5)

and speed of sound

$$c_s = \sqrt{c/3} \tag{6}$$

In general, a discreet velocity Boltzmann-BGK equation (DVBE) can be written in component form as

$$\frac{\partial f_i}{\partial t} + u_i \frac{\partial f_i}{\partial x} + v_i \frac{\partial f_i}{\partial y} = -\frac{1}{\lambda} \left(f_i - f_i^{eq} \right) \tag{7}$$

where f_i is the distribution function for velocity $\boldsymbol{\xi}_i = (u_i, v_i)$.

In discretized velocity space, the macroscopic density and momentum are given by:

$$\rho = \sum_{j=1}^{N} f_j \tag{8}$$

$$\rho \boldsymbol{u} = \sum_{j=1}^{N} f_j \boldsymbol{\xi}_j \tag{9}$$

where N is the number of discreet velocities.

If we define $\mathbf{f} = (f_1, f_2, ..., f_N)$, we can write Eq. (7) in matrix form as

$$\frac{\partial \mathbf{f}}{\partial t} + \mathbf{A} \frac{\partial \mathbf{f}}{\partial x} + \mathbf{B} \frac{\partial \mathbf{f}}{\partial y} = -\frac{1}{\lambda} \left(\mathbf{f} - \mathbf{f}^{eq} \right)$$
(10)

where **A** and **B** are diagonal matrices such that $A_{ii} = u_i$ and $B_{ii} = v_i$.

III. Linear Analysis of Boltzmann BGK Equation

We first investigate the linear waves supported by the discreet velocity Boltzmann-BGK equation. A similar study for a 3D DVBE has been conducted in a recent work in Ref. 18.

To perform a linear analysis of Eq. (7) or Eq. (10), we first separate the distribution function into a uniform mean flow component and a perturbation component as

$$f_i = \bar{f}_i^{eq} + f_i' \tag{11}$$

where the overbar and the prime sign denote the mean and the perturbation values, respectively. Redefining the right side of Eq. (7) as $g_i(f_j)$ and linearizing it yields

$$g_i(f_j) = g_i(\bar{f}_j^{eq}) + \frac{\partial g_i}{\partial f_j}(\bar{f}_j^{eq})f_j' + O(f_j'^2)$$
(12)

Noting that

$$\frac{\partial g_i}{\partial f_i}(\bar{f}_j^{eq}) = -\frac{1}{\lambda} \left(\delta_{ij} - \frac{\partial f_i^{eq}}{\partial f_i}(\bar{f}_j^{eq}) \right) f_i' \tag{13}$$

and that $g_i(\bar{f}_j^{eq})=0$ and plugging back into Eq. (7) gives

$$\frac{\partial f'_{i}}{\partial t} + \boldsymbol{\xi}_{i} \cdot \nabla f'_{i} = -\frac{1}{\lambda} \left(\delta_{ij} - \frac{\partial f_{i}^{eq}}{\partial f_{i}} (\bar{f}_{j}^{eq}) \right) f'_{i} \tag{14}$$

The two dimensional form of the above can be written in matrix form as

$$\frac{\partial \mathbf{f'}}{\partial t} + \mathbf{A} \frac{\partial \mathbf{f'}}{\partial x} + \mathbf{B} \frac{\partial \mathbf{f'}}{\partial y} = -\frac{1}{\lambda} (\mathbf{I} - \mathbf{J}) \mathbf{f'}$$
(15)

where I is the identity matrix and J is defined by $J_{ij} = \frac{\partial f_i^{eq}}{\partial f_j} (\bar{f}_j^{eq})$.

We look for plane wave solutions $f'(x,t) = \hat{f}e^{i\mathbf{k}\cdot\mathbf{x}-i\omega t}$ and we obtain an eigenvalue problem for ω with given values of k_x and k_y , as follows:

$$-i\omega\hat{\mathbf{f}} + ik_x \mathbf{A}\hat{\mathbf{f}} + ik_y \mathbf{B}\hat{\mathbf{f}} = -\frac{1}{\lambda}(\mathbf{I} - \mathbf{J})\hat{\mathbf{f}}$$
(16)

or equivalently

$$\omega \hat{\mathbf{f}} = M \hat{\mathbf{f}} \tag{17}$$

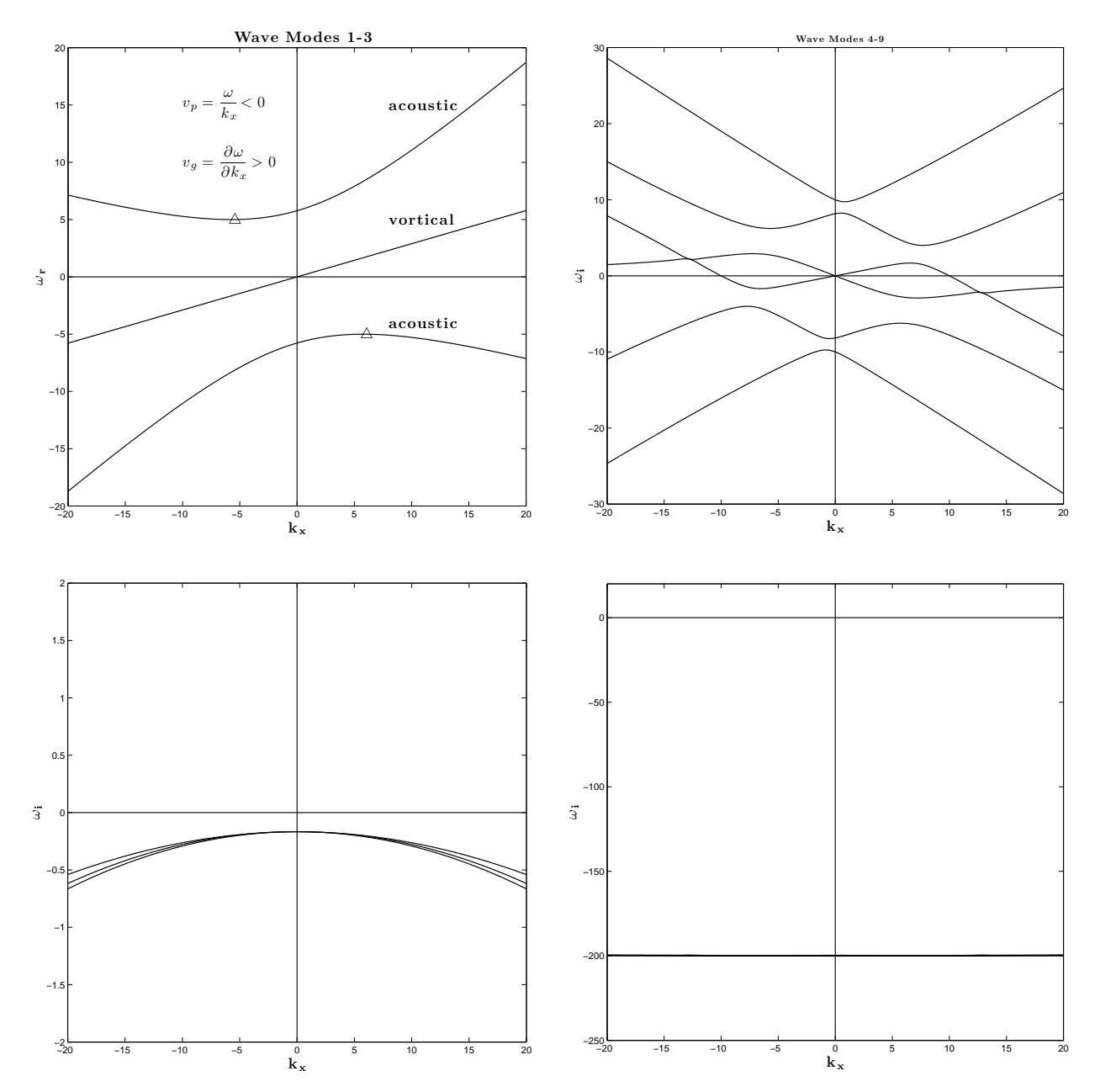


Figure 1. Dispersion relations of all linear waves supported by Eq. (17).

where
$$\mathbf{M} := k_x \mathbf{A} + k_y \mathbf{B} - \frac{i}{\lambda} (\mathbf{I} - \mathbf{J})$$

The eigenvalue problem in Eq. (17) will be solved numerically. Using the D2Q9 model as an example, Figure 1 shows the dispersion relations of ω v.s. k_x for all the nine wave modes, with $k_y=10$, $\lambda=0.005$ and the mean flow velocity $U_0=0.5c_s$. The nine eigenvalues shown can be divided into two groups. One group of modes, shown in the left side of Figure 1, consist of three hydrodynamic waves, namely the two acoustic modes and one vortical mode. The imaginary parts of the three modes are negative, showing a damping effect of the viscosity in the BGK model. The other group of modes, shown on the right side of Figure 1, have significantly higher damping rates.

It has been verified that dispersion relations of the three hydrodynamic waves, for the real part of ω , follow closely the curves given by

$$D_a(\omega, k_x, k_y) = (\omega - U_0 k_x)^2 - c_s^2 (k_x^2 + k_y^2) = 0$$
(18)

for the acoustic waves and

$$D_v(\omega, k_x, k_y) = \omega - U_0 k_x = 0 \tag{19}$$

for the vortical wave. These are the dispersion relations for the linearized Euler equations. These findings are similar to those reported in Ref. 18.

IV. PML Derivation

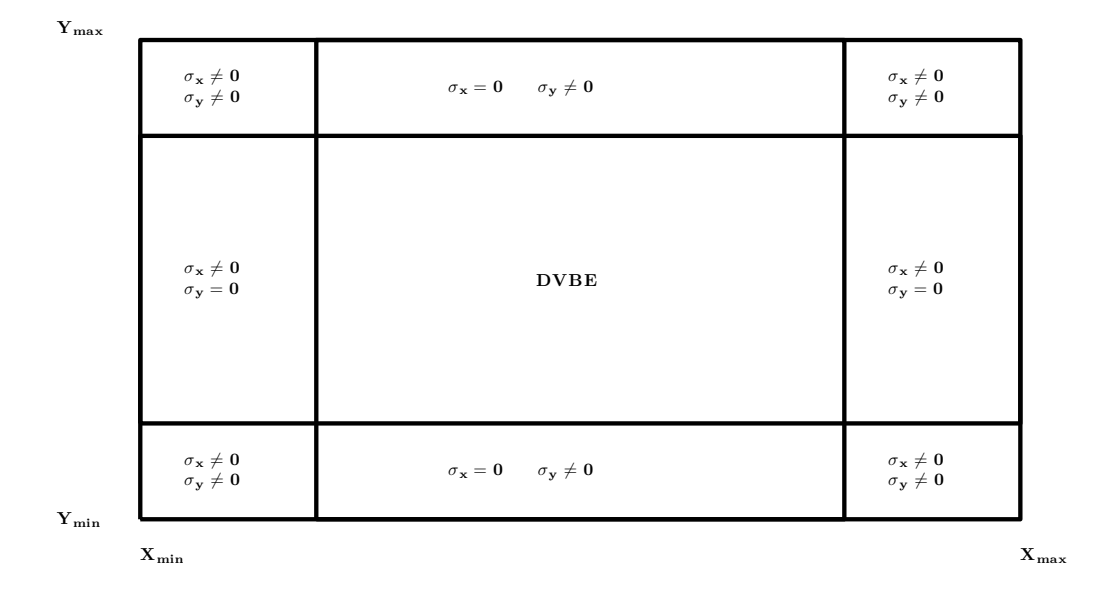


Figure 2. Illustration of a computational domain combining the DVBE and PML domains.

The PML technique involves a complex change of variables in the frequency domain. $^{10,\,19}$ A requirement for stability is that the waves have consistent phase and group velocity. In the case of Euler equations, the inconsistency can be corrected by a proper space-time transformation in the derivation process. $^{10,\,11,\,20,\,21}$

The acoustic wave modes in Figure 1 would similarly exhibit inconsistent phase and group velocities when the mean velocity U_0 is not zero. The symbols in Figure 1 denote the location where the group velocity is zero, indicating that parts of the dispersion curves have inconsistent phase and group velocities, namely, a negative phase velocity but a positive group velocity for the waves that lie between the location of the symbol and the vertical axis. However, as has been demonstrated in previous studies, these inconsistencies in the phase and group velocities can be corrected by a proper linear space-time transformation of the form

$$\bar{t} = t + \beta x \tag{20}$$

where β is defined by

$$\beta = -\frac{k_x^*}{\omega^*} \tag{21}$$

in which k_x^* and ω^* are the roots of

$$D_a(\omega^*, k_x^*, k_y) = 0, \quad \text{and} \quad \frac{\partial D_a}{\partial k_x}(\omega^*, k_x^*, k_y) = 0$$
(22)

By Eqs. (18) and (22), we find that, for any k_y , $\omega^* = [(U_0^2 - c_s^2)]/U_0]k_x^*$ which leads to

$$\beta = -\frac{U_0}{c_s^2 - U_0^2} \tag{23}$$

For the second group of waves, the inconsistencies of phase and group velocities are also found but cannot be corrected easily. However, with intrinsic high damping rates associated with these modes, the application of PML change of variables may not cause instability when the PML absorption coefficients are not exceedingly large.

To derive the PML, we assume a mean flow with velocity U_0 and we decompose the distribution functions into a uniform mean flow component and a perturbation component

$$f = \bar{f} + f' \tag{24}$$

where the overbar and the prime sign denote the steady mean and the perturbation values, respectively. We also assume that $\bar{f} = \bar{f}^{eq}$ and the mean flow equilibrium distribution function, \bar{f} , satisfies the time-indepedent equation

$$A\frac{\partial \bar{f}}{\partial x} + B\frac{\partial \bar{f}}{\partial y} = 0 \tag{25}$$

We will derive the absorbing equation for the perturbation distribution function f':

$$\frac{\partial \mathbf{f'}}{\partial t} + \mathbf{A} \frac{\partial (\mathbf{f} - \bar{\mathbf{f}})}{\partial x} + \mathbf{B} \frac{\partial (\mathbf{f} - \bar{\mathbf{f}})}{\partial y} = -\frac{1}{\lambda} (\mathbf{f} - \mathbf{f}^{eq})$$
(26)

Two formulations will be given below, following the work in Ref. 22.

IV.A. Unsplit Formulation

To derive the PML equation for f', we first apply a space-time transformation,

$$\bar{t} = t + \beta x \tag{27}$$

where β is given in Eq. (23). Equation (26) becomes

$$\frac{\partial \mathbf{f'}}{\partial \bar{t}} + \beta \mathbf{A} \frac{\partial (\mathbf{f} - \bar{\mathbf{f}})}{\partial \bar{t}} + \mathbf{A} \frac{\partial (\mathbf{f} - \bar{\mathbf{f}})}{\partial x} + \mathbf{B} \frac{\partial (\mathbf{f} - \bar{\mathbf{f}})}{\partial y} = -\frac{1}{\lambda} (\mathbf{f} - \mathbf{f}^{eq})$$
(28)

Writing the above in the frequency domain and applying the PML complex change of variables as in Ref. 10 yields

$$(-i\omega)\hat{\mathbf{f}'} + (-i\omega)\beta \mathbf{A}(\mathbf{f} - \bar{\mathbf{f}}) + \mathbf{A}\frac{1}{1 + \frac{i\sigma_x}{\omega}} \frac{\partial (\mathbf{f} - \bar{\mathbf{f}})}{\partial x} + \mathbf{B}\frac{1}{1 + \frac{i\sigma_y}{\omega}} \frac{\partial (\mathbf{f} - \bar{\mathbf{f}})}{\partial y} = -\frac{1}{\lambda}(\mathbf{f} - \mathbf{f}^{eq})$$
(29)

To write the above in the time-domain, we multiply Eq. (29) by $\left(1 + \frac{i\sigma_x}{\omega}\right) \left(1 + \frac{i\sigma_y}{\omega}\right)$ to obtain

$$(-i\omega)\hat{\mathbf{f}'} + (\sigma_x + \sigma_y)\hat{\mathbf{f}'} + \sigma_x\sigma_y\frac{i}{\omega}\hat{\mathbf{f}'} + (-i\omega)\beta\mathbf{A}(\mathbf{f} - \bar{\mathbf{f}}) + (\sigma_x + \sigma_y)\beta\mathbf{A}(\mathbf{f} - \bar{\mathbf{f}}) + \sigma_x\sigma_y\frac{i}{\omega}\beta\mathbf{A}(\mathbf{f} - \bar{\mathbf{f}})$$

$$+ \mathbf{A}\left(1 + \frac{i\sigma_y}{\omega}\right)\frac{\partial(\mathbf{f} - \bar{\mathbf{f}})}{\partial x} + \mathbf{B}\left(1 + \frac{i\sigma_x}{\omega}\right)\frac{\partial(\mathbf{f} - \bar{\mathbf{f}})}{\partial y} = -\frac{1}{\lambda}\left(1 + \frac{i\sigma_x}{\omega} + \frac{i\sigma_y}{\omega} - \frac{\sigma_x\sigma_y}{\omega^2}\right)\left(\mathbf{f} - \bar{\mathbf{f}}^{eq}\right)$$
(30)

We can write the above back in the time domain by introducing auxiliary variables q, r_1 and r_2 such that

$$\frac{\partial \mathbf{q}}{\partial t} = \mathbf{f} - \bar{\mathbf{f}}, \qquad \frac{\partial \mathbf{r}_1}{\partial t} = \mathbf{f} - \mathbf{f}^{eq}, \qquad \frac{\partial \mathbf{r}_2}{\partial t} = \mathbf{r}_1$$
 (31)

In the original physical space and time, the PML absorbing equation can finally be written as

$$\frac{\partial \mathbf{f}}{\partial t} + \mathbf{A} \frac{\partial \mathbf{f}}{\partial x} + \mathbf{B} \frac{\partial \mathbf{f}}{\partial y} + \sigma_y \mathbf{A} \frac{\partial \mathbf{q}}{\partial x} + \sigma_x \mathbf{B} \frac{\partial \mathbf{q}}{\partial y} + (\sigma_x + \sigma_y) (\mathbf{f} - \bar{\mathbf{f}}) + \sigma_x \sigma_y \mathbf{q}
+ \sigma_x \beta \mathbf{A} \left[(\mathbf{f} - \bar{\mathbf{f}}) + \sigma_y \mathbf{q} \right] = -\frac{1}{\lambda} (\mathbf{f} - \mathbf{f}^{eq}) - \frac{1}{\lambda} (\sigma_x + \sigma_y) \mathbf{r}_1 - \frac{1}{\lambda} \sigma_x \sigma_y \mathbf{r}_2$$
(32)

IV.B. Split Formulation

To derive the split PML equations, we start with Eq. (29) and we introduce auxiliary variables q_1 , q_2 and q_3 which satisfy the following equations

$$(-i\omega)\hat{\mathbf{q}}_1 + (-i\omega)\beta \mathbf{A}(\mathbf{f} - \bar{\mathbf{f}}) + \frac{1}{1 + \frac{i\sigma_x}{\omega}} \mathbf{A} \frac{\partial (\mathbf{f} - \bar{\mathbf{f}})}{\partial x} = 0$$
(33)

$$(-i\omega)\hat{\mathbf{q}}_2 + \frac{1}{1 + \frac{i\sigma_y}{\alpha}} \mathbf{B} \frac{\partial (\mathbf{f} - \bar{\mathbf{f}})}{\partial y} = 0$$
(34)

$$(-i\omega)\hat{\mathbf{q}}_3 = -\frac{1}{\lambda} \left(\hat{\mathbf{f}} - \hat{\mathbf{f}}^{eq} \right) \tag{35}$$

Eq. (29) is recovered where $\hat{f}' = \hat{q}_1 + \hat{q}_2 + \hat{q}_3$.

Multiplying Eqs. (33) and (34) by $\left(1 + \frac{i\sigma_x}{\omega}\right)$ and $\left(1 + \frac{i\sigma_y}{\omega}\right)$ respectively, we obtain

$$(-i\omega)\hat{\mathbf{q}}_1 + \sigma_x\hat{\mathbf{q}}_1 + \sigma_x\beta \mathbf{A}(\mathbf{f} - \bar{\mathbf{f}}) + (-i\omega)\beta \mathbf{A}(\mathbf{f} - \bar{\mathbf{f}}) + \mathbf{A}\frac{\partial(\mathbf{f} - \bar{\mathbf{f}})}{\partial x} = 0$$
(36)

$$(-i\omega)\hat{\mathbf{q}}_2 + \sigma_y\hat{\mathbf{q}}_2 + B\frac{\partial(\mathbf{f} - \bar{\mathbf{f}})}{\partial y} = 0$$
(37)

$$(-i\omega)\hat{\mathbf{q}}_3 = -\frac{1}{\lambda} \left(\hat{\mathbf{f}} - \hat{\mathbf{f}}^{eq} \right) \tag{38}$$

Changing the above back to the original time domain gives

$$\frac{\partial \mathbf{q}_1}{\partial t} + \sigma_x \mathbf{q}_1 + \sigma_x \beta \mathbf{A} (\mathbf{f} - \bar{\mathbf{f}}) + \mathbf{A} \frac{\partial (\mathbf{f} - \bar{\mathbf{f}})}{\partial x} = 0$$
(39)

$$\frac{\partial \mathbf{q}_2}{\partial t} + \sigma_y \mathbf{q}_2 + \mathbf{B} \frac{\partial (\mathbf{f} - \bar{\mathbf{f}})}{\partial u} = 0 \tag{40}$$

$$\frac{\partial q_3}{\partial t} = -\frac{1}{\lambda} \left(\mathbf{f} - \mathbf{f}^{eq} \right) \tag{41}$$

By adding Eqs. (39), (40), and (41) we obtain the equation for f and a second, split, PML set of equations

$$\frac{\partial \mathbf{f}}{\partial t} + \mathbf{A} \frac{\partial \mathbf{f}}{\partial x} + \mathbf{B} \frac{\partial \mathbf{f}}{\partial y} + \sigma_x \mathbf{q}_1 + \sigma_y \mathbf{q}_2 + \sigma_x \beta \mathbf{A} (\mathbf{f} - \bar{\mathbf{f}}) = -\frac{1}{\lambda} (\mathbf{f} - \mathbf{f}^{eq})$$
(42)

$$\frac{\partial \mathbf{q}_1}{\partial t} + \sigma_x \mathbf{q}_1 + \sigma_x \beta \mathbf{A} (\mathbf{f} - \bar{\mathbf{f}}) + \mathbf{A} \frac{\partial (\mathbf{f} - \bar{\mathbf{f}})}{\partial x} = 0$$
(43)

$$\frac{\partial \mathbf{q}_2}{\partial t} + \sigma_y \mathbf{q}_2 + \mathbf{B} \frac{\partial (\mathbf{f} - \bar{\mathbf{f}})}{\partial y} = 0 \tag{44}$$

In component form we have

$$\frac{\partial f_i}{\partial t} + u_i \frac{\partial f_i}{\partial x} + v_i \frac{\partial f_i}{\partial y} + \sigma_x q_{1i} + \sigma_y q_{2i} + \sigma_x \beta u_i (f_i - \bar{f_i}) = -\frac{1}{\lambda} (f_i - f_i^{eq})$$
(45)

$$\frac{\partial q_{1i}}{\partial t} + \sigma_x q_{1i} + \sigma_x \beta u_i (f_i - \bar{f}_i) + u_i \frac{\partial (f_i - \bar{f}_i)}{\partial x} = 0$$
(46)

$$\frac{\partial q_{2i}}{\partial t} + \sigma_y q_{2i} + v_i \frac{\partial (f_i - \bar{f}_i)}{\partial y} = 0 \tag{47}$$

We note that the split formulation does not require additional spatial derivatives. On the other hand, the unsplit formulation ensures that $f = \bar{f}$ when $\frac{\partial q}{\partial t} = 0$.

V. Linear Analysis of DVBE PML

In this section, we study the linear stability of the PML absorbing equations proposed in the previous section. A linear analysis of the split PML Eqs. (42)-(44) gives the following eigenvalue problem:

$$\omega \hat{\mathbf{f}} = \mathbf{M}_1 \hat{\mathbf{f}} - i\sigma_x \hat{\mathbf{q}}_1 - i\sigma_y \hat{\mathbf{q}}_2 \tag{48}$$

$$\omega \hat{\mathbf{q}}_1 = [k_x - i\sigma_x \beta] \, \mathbf{A}\hat{\mathbf{f}} - i\sigma_x \hat{\mathbf{q}}_1 \tag{49}$$

$$\omega \hat{\mathbf{q}}_2 = k_y B \hat{\mathbf{f}} - i \sigma_y \hat{\mathbf{q}}_2 \tag{50}$$

where $M_1 := k_x A + k_y B - \frac{i}{\lambda} (I - J) - i \sigma_x \beta A$. The eigen solutions of the unsplit formulation are equivalent to those of the split formulation.

The occurrence of any eigenvalue ω with a positive imaginary part ω_i will indicate instability. On the other hand, if all the eigenvalues have nonpositive imaginary parts, then the system is stable. In Figure 3, we plot the contours of maximum ω_i of all eigenvalues for $0 \le M = U_0/c_s \le 0.7$, $-3.15 \le k_x, k_y \le 3.15$, and $0 \le \sigma_x, \sigma_y \le 10$, using again the D2Q9 as an example. The imaginary part of ω is negative for the σ_x layer and small enough to be considered zero for the other two layers. This indicates that the proposed PML equations are stable for the range of values considered for M, σ_x , σ_y , k_x and k_y .

VI. Numerical Methods

VI.A. Finite Difference Solution

The discreet velocity Boltzmann-BGK Eq. (10) and the PML absorbing Eqs. (42)-(44) will be solved by a finite difference scheme. The spatial derivative terms will be discretized by the DRP scheme²³ and Runge-Kutta (RK) schemes are used for the time integration. Due to the stiffness of the collision term, explicit RK schemes resulted in an exceedingly small time step Δt . To increase the efficiency of time integration, we use additive implicit-explicit (IMEX) RK schemes.^{12–14} If we write the DVBE as

$$\frac{\partial f}{\partial t} = h(f) + \frac{1}{\lambda}g(f)$$

where h(f) denotes symbolically all the non-collision terms and g(f) denotes the part in the collision term, the IMEX numerical scheme for solution f^n at time t_n to advance to f^{n+1} at time $t_n + \Delta t$ is

$$f^{n+1} = f^n + \Delta t \sum_{i=1}^{\nu} \tilde{w}_i h(f^{(i)}) + \frac{\Delta t}{\lambda} \sum_{i=1}^{\nu} w_i g(f^{(i)})$$
(51)

where the stage values $f^{(i)}$ are given by

$$f^{(1)} = f^n + \frac{\Delta t}{\lambda} a_{11} g(f^{(1)}), \tag{52}$$

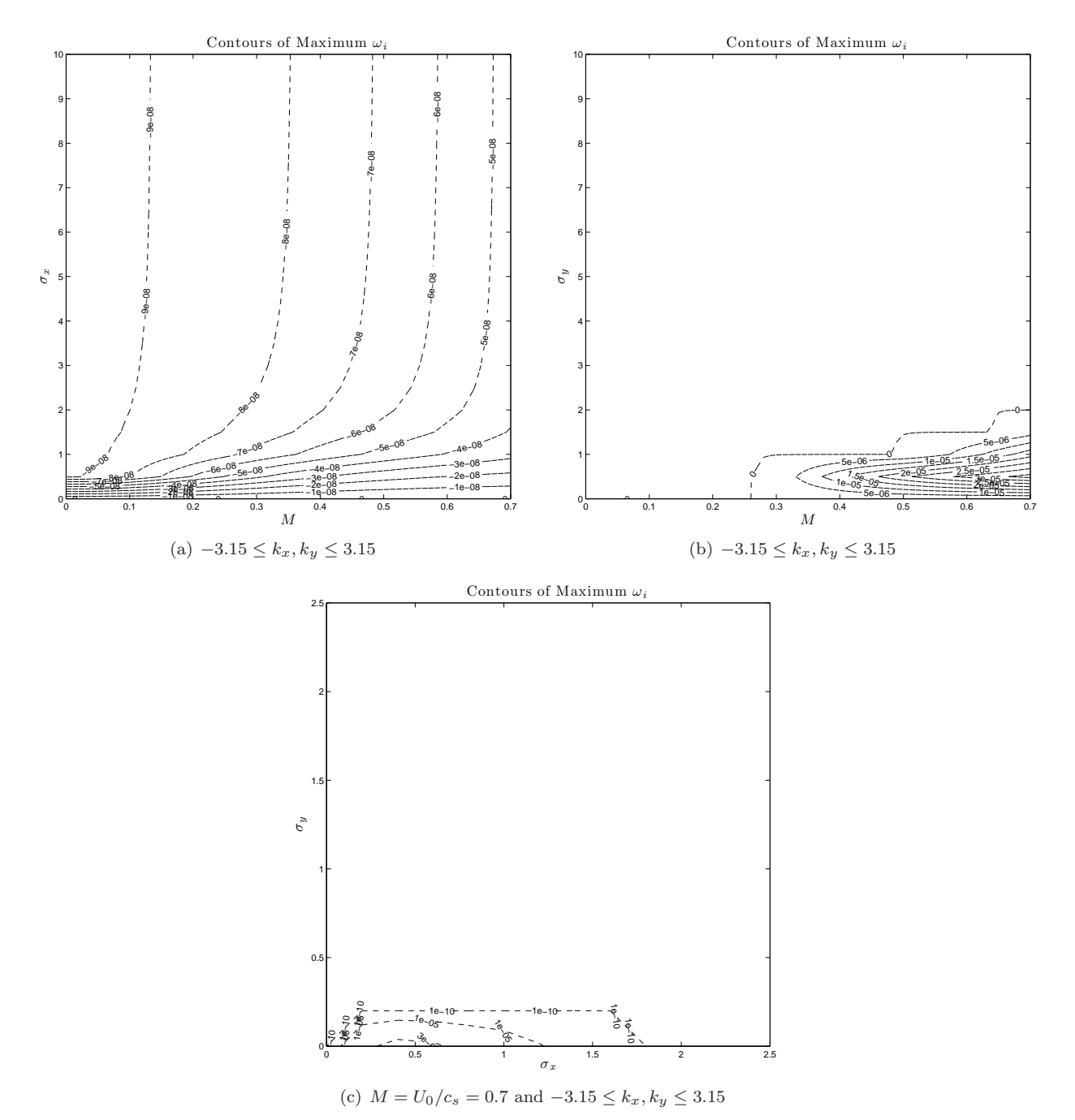


Figure 3. Contours of maximum ω_i for $\lambda=0.00011,~0\leq M=U_0/c_s\leq 0.7$ and $-3.15\leq k_x,k_y\leq 3.15$.

$$f^{(i)} = f^n + \Delta t \sum_{j=1}^{i-1} \tilde{a}_{ij} h(f^{(j)}) + \frac{\Delta t}{\lambda} \sum_{j=1}^{i} a_{ij} g(f^{(j)}), \quad i = 2, 3, ..., \nu.$$
 (53)

The coefficients \tilde{a}_{ij} , \tilde{w}_i , a_{ij} , and w_i are given in a double Butcher's tableau as follows

$$\begin{array}{c|c} \tilde{c} & \tilde{A} \\ \hline & \tilde{w}^T \end{array} \qquad \begin{array}{c|c} c & A \\ \hline & w \end{array}$$

Some second-, third- and fourth-order IMEX Runge-Kutta schemes are: IMEX2 Second-order scheme: $^{12}\,$

IMEX3 Third-order scheme:¹²

where $\alpha = 0.24169426078821$, $\beta = 0.06042356519705$, and $\eta = 0.1291528696059$.

IMEX4 Fourth-order scheme:²⁴

ARK4(3)6L[2]SA-ERK (Explicit)

0	0	0	0	0	0	0
$\frac{1}{2}$	$\frac{1}{2}$	0	0	0	0	0
$\frac{83}{250}$	$\frac{13861}{62500}$	$\frac{6889}{62500}$	0	0	0	0
$\frac{31}{50}$	$\frac{-116923316275}{2393684061468}$	$\frac{-2731218467317}{15368042101831}$	9408046702089 11113171139209	0	0	0
$\frac{17}{20}$	$\frac{-451086348788}{2902428689909}$	$\frac{-2682348792572}{7519795681897}$	12662868775082 11960479115383	$\frac{3355817975965}{11060851509271}$	0	0
1	$\frac{647845179188}{3216320057751}$	73281519250 8382639484533	552539513391 3454668386233	3354512671639 8306763924573	$\frac{4040}{17871}$	0
	82889 524892	0	15625 83664	69875 102672	$\frac{-2260}{8211}$	$\frac{1}{4}$

ARK4(3)6L[2]SA-ESDIRK (Implicit)

0	0	0	0	0	0	0
$\frac{1}{2}$	$\frac{1}{4}$	$\frac{1}{4}$	0	0	0	0
$\frac{\frac{1}{2}}{83}$ $\frac{83}{250}$	$\frac{8611}{62500}$	$\frac{-1743}{31250}$	$\frac{1}{4}$	0	0	0
$\frac{31}{50}$	$\frac{5012029}{34652500}$	$\frac{-654441}{2922500}$	$\frac{174375}{388108}$	$\frac{1}{4}$	0	0
$\frac{17}{20}$	$\frac{15267082809}{155376265600}$	$\frac{-71443401}{120774400}$	$\frac{730878875}{902184768}$	$\frac{2285395}{8070912}$	$\frac{1}{4}$	0
1	$\frac{82889}{524892}$	0	$\frac{15625}{83664}$	$\frac{69875}{102672}$	$\frac{-2260}{8211}$	$\frac{1}{4}$
	$\frac{82889}{524892}$	0	$\frac{15625}{83664}$	$\frac{69875}{102672}$	$\frac{-2260}{8211}$	$\frac{1}{4}$

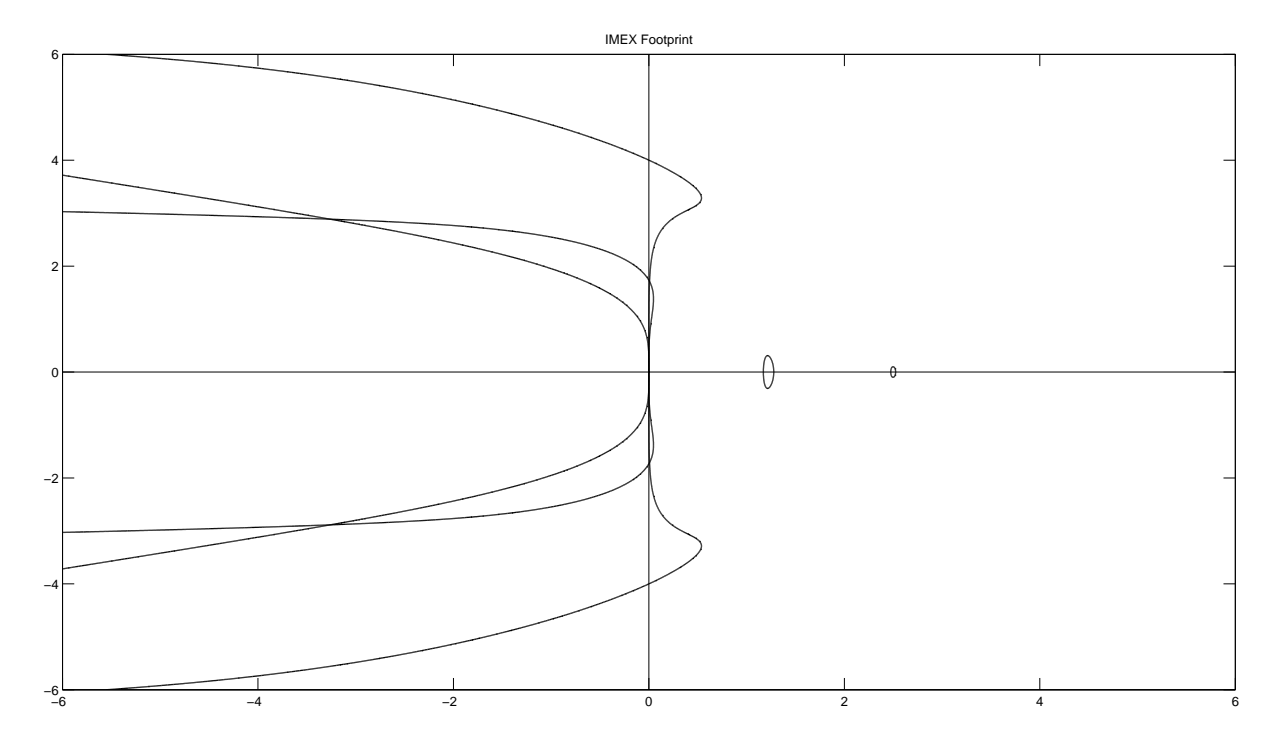


Figure 4. IMEX Footprints for IMEX 2, IMEX3 and IMEX 4.

Figure 4 shows the footprints of the three IMEX schemes. With each additional order, the IMEX schemes enlarge their stability region so that IMEX 4 has the largest stability region of the three.

Although the IMEX RK scheme has implicit steps, due to the special structure of the BGK collision operator, the implicit step can be solved explicitly. To solve the implicit step for $f^{(i)}$, we follow the method used by Pieraccini and Puppo in Ref. 12 and first compute ρ and \boldsymbol{u} by taking the moments of Eq. (53). This reduces to taking the moments of $f^n + \Delta t \sum_{j=1}^{i-1} \tilde{a}_{ij} h(f^{(j)})$ as the collisional invariants make the other terms drop out. Then $f^{(i)eq}$ is given by Eq. (4), and $f^{(i)}$ can be calculated explicitly from Eq. (53).

VI.B. LBM Solution

The lattice discretization of the Boltzmann-BGK Eq. (7) can be written as

$$f_i(\boldsymbol{x} + \boldsymbol{\xi}_i \Delta t, t + \Delta t) - f_i(\boldsymbol{x}, t) = -\frac{\Delta t}{\lambda + \frac{\Delta t}{2}} (f_i(\boldsymbol{x}, t) - f_i^{eq}(\boldsymbol{x}, t))$$
(54)

and the lattice discretization of the PML Eqs. (42), (43), and (44) is

$$f_{i}(\boldsymbol{x} + \boldsymbol{\xi}_{i}\Delta t, t + \Delta t) - f_{i}(\boldsymbol{x}, t) = -\frac{\Delta t}{\lambda + \frac{\Delta t}{2}} (f_{i}(\boldsymbol{x}, t) - f_{i}^{eq}(\boldsymbol{x}, t)) - \Delta t \sigma_{x} q_{1i}(\boldsymbol{x}, t) - \Delta t \sigma_{y} q_{2i}(\boldsymbol{x}, t)$$

$$- \Delta t \sigma_{x} \beta u_{i} (f_{i}(\boldsymbol{x}, t) - \bar{f}_{i}^{eq}(\boldsymbol{x}, t))$$

$$(55)$$

$$q_{1i}(\boldsymbol{x}, t + \Delta t) - q_{1i}(\boldsymbol{x}, t) = -\Delta t \sigma_x q_{1i}(\boldsymbol{x}, t) - \Delta t u_i \frac{\partial (f_i(\boldsymbol{x}, t) - \bar{f}_i^{eq}(\boldsymbol{x}, t))}{\partial x} - \Delta t \sigma_x \beta u_i (f_i(\boldsymbol{x}, t) - \bar{f}_i^{eq}(\boldsymbol{x}, t))$$
(56)

$$q_{2i}(\boldsymbol{x}, t + \Delta t) - q_{2i}(\boldsymbol{x}, t) = -\Delta t \sigma_y q_{2i}(\boldsymbol{x}, t) - \Delta t v_i \frac{\partial (f_i(\boldsymbol{x}, t) - \bar{f}_i^{eq}(\boldsymbol{x}, t))}{\partial y}$$
(57)

The spatial derivative terms in the above will be discretized by the DRP scheme and the Euler forward method is used for the time integration.

A linear analysis of the above lattice PML equations gives the following eigenvalue problem:

$$\hat{\mathbf{f}}e^{-i\omega\Delta t} = \mathbf{C}\left[\mathbf{I} - \frac{\Delta t}{\lambda + \frac{\Delta t}{2}}(\mathbf{I} - \mathbf{J}) - \Delta t\sigma_x \beta \mathbf{A}\right]\hat{\mathbf{f}} - \Delta t\sigma_x \mathbf{C}\hat{\mathbf{q}}_1 - \Delta t\sigma_y \mathbf{C}\hat{\mathbf{q}}_2$$
(58)

$$\hat{\mathbf{q}}_{1}e^{-i\omega\Delta t} = \left[-ik_{x}\Delta t - \Delta t\sigma_{x}\beta\right]\mathbf{A}\hat{\mathbf{f}} + \left[1 - \Delta t\sigma_{x}\right]\hat{\mathbf{q}}_{1}$$
(59)

$$\hat{\mathbf{q}}_{2}e^{-i\omega\Delta t} = -ik_{y}\Delta t \mathbf{B}\hat{\mathbf{f}} + [1 - \Delta t\sigma_{y}]\hat{\mathbf{q}}_{2}$$
(60)

where C is the diagonal matrix defined as $C_{jj} = e^{-i\mathbf{k}\cdot\mathbf{\xi}_j\Delta t}$ and the matrices I, A, B and J are as previously defined.

Solutions of the PML equations in a lattice scheme will be presented in a future work.

VII. Numerical Examples

VII..1. Acoustic Wave

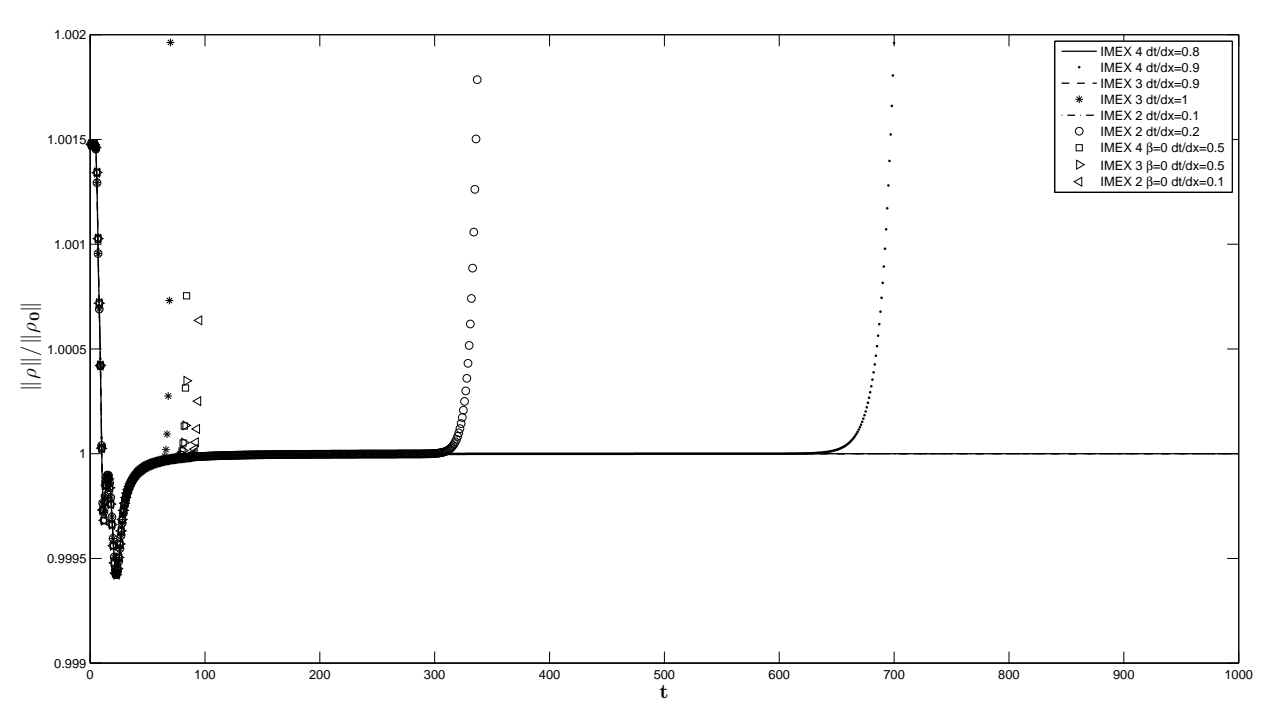


Figure 5. IMEX stability for $\epsilon = 0.1$, $r = 8\Delta x$, M = 0.5, $\sigma_x \Delta x = \sigma_y \Delta y = 1$ and $D = 20\Delta x$.

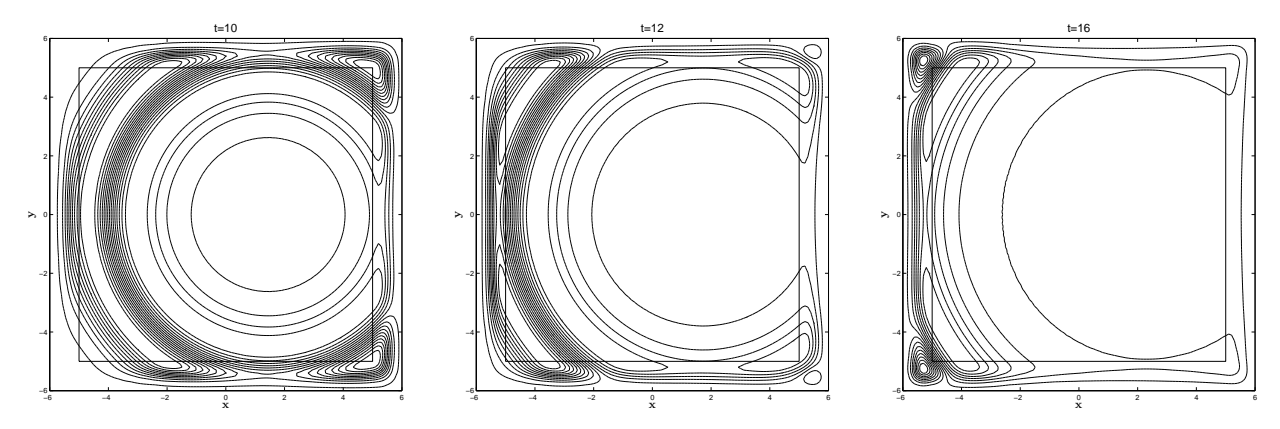


Figure 6. IMEX 3 density contours for $\epsilon=0.01,\ r=8\Delta x,\ M=0.25,\ \sigma_x\Delta x=\sigma_y\Delta y=1$ and $D=10\Delta x$.

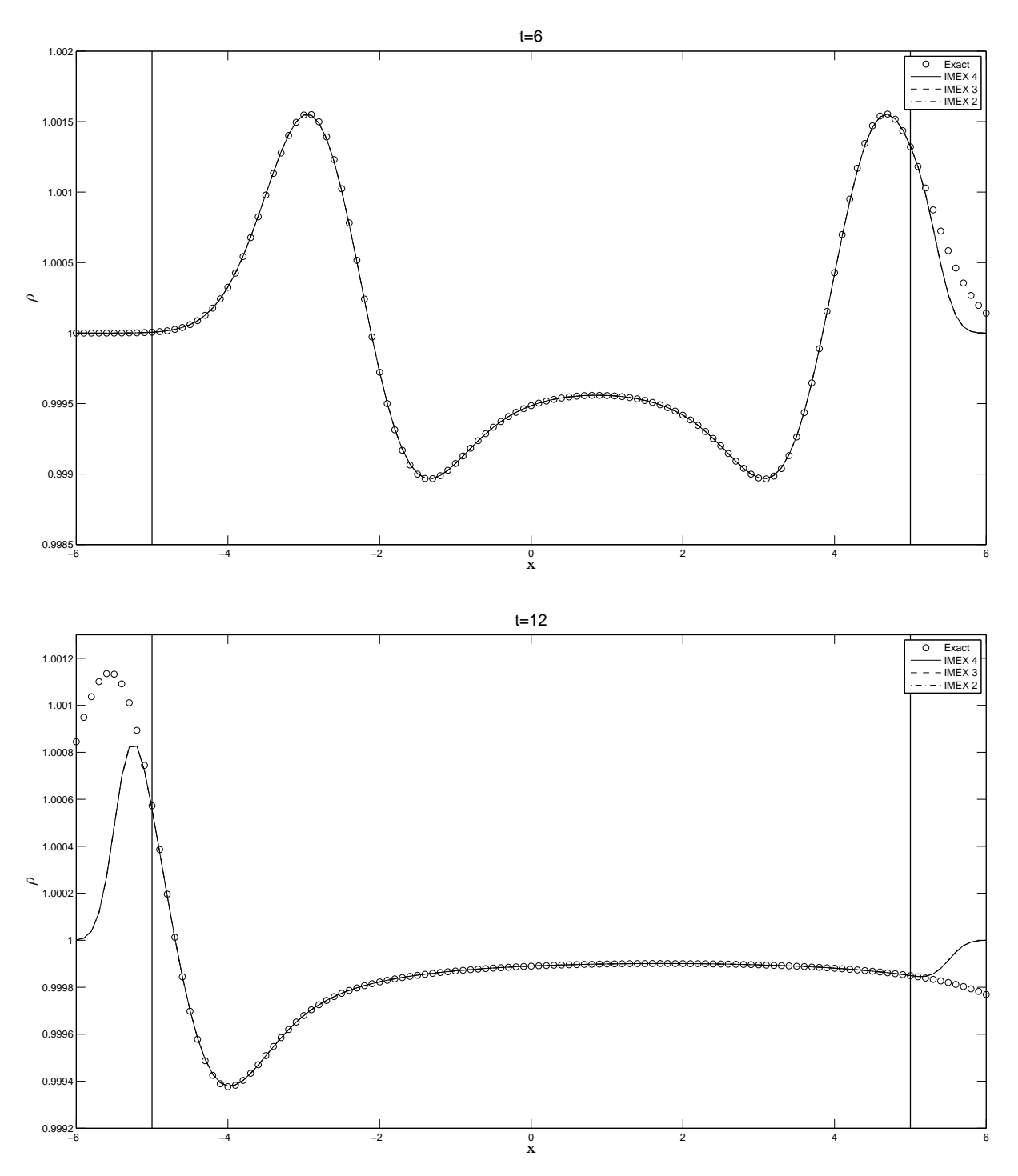


Figure 7. Comparison of IMEX numerical solutions with exact solution for $\epsilon=0.01,\,r=8\Delta x,\,M=0.25,\,\sigma_x\Delta x=\sigma_y\Delta y=1$ and $D=10\Delta x.$

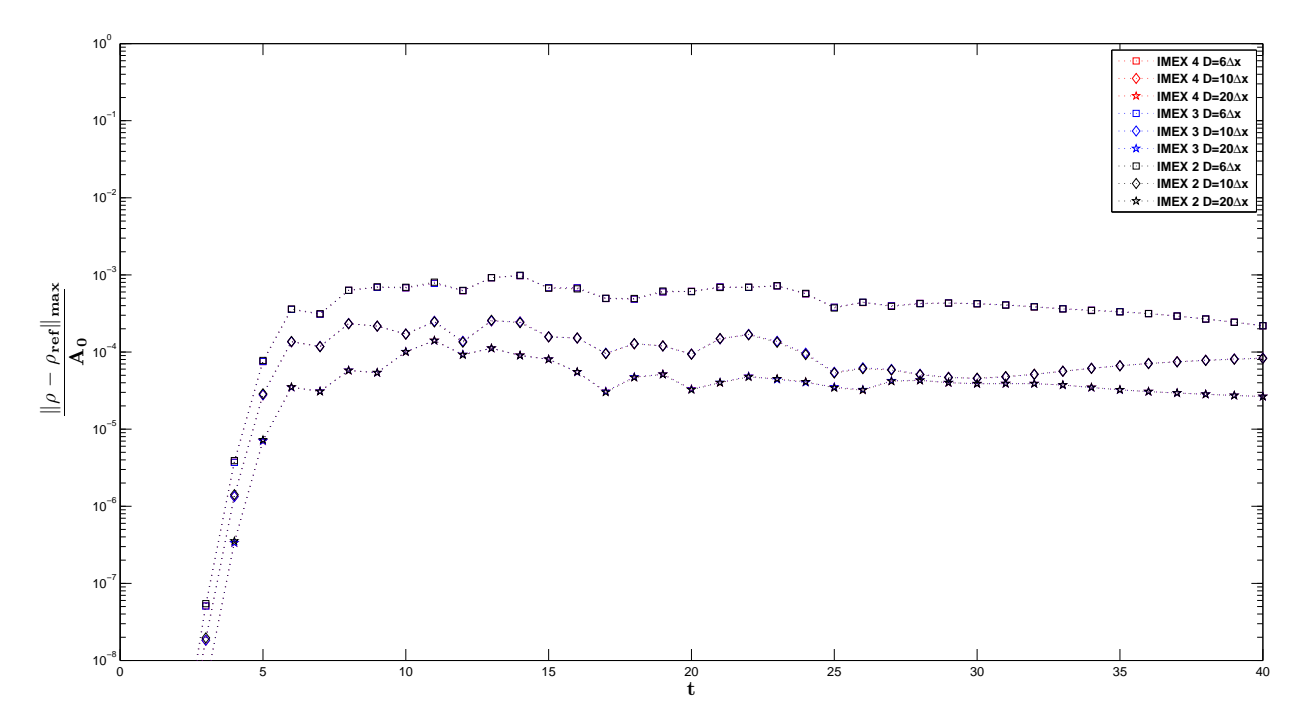


Figure 8. Acoustic reflection coefficient for $\epsilon = 0.01$, $r = 8\Delta x$, M = 0.25, and $\sigma_x \Delta x = \sigma_y \Delta y = 1$. $A_0 = 0.0015$.

We test the PML equations by simulating a Gaussian acoustic pulse in a mean flow with Mach number M. The initial conditions for density ρ and velocity components u and v are:

$$\rho = 1 + \epsilon \exp\left[-(\ln 2)\frac{x^2 + y^2}{r^2}\right]$$

$$u = Mc_s$$

$$v = 0$$
(61)

For the finite difference solution of the PML Eqs. (42)-(44), we use a computational domain of [-5,5] x [-5,5] and a uniform grid with $\Delta x = \Delta y = 0.1$. The PML domains extend further by a width D to absorb the outgoing waves as shown in Figure 2.

The use of absorption coefficients σ_x and σ_y in the PML layers is illustrated in Figure 2. The rate of absorption varies with space as

$$\sigma_x = \sigma_m \left| \frac{x - x_0}{D} \right|^2, \quad \sigma_y = \sigma_m \left| \frac{y - y_0}{D} \right|^2$$
 (62)

where x_0 and y_0 are the locations of the DVBE/PML interfaces and σ_m is chosen so that $1 \le \sigma_m \Delta x \le 2$.

The distribution functions f_i are initialized using the equilibrium values obtained from the above macroscopic variables ρ and \boldsymbol{u} . The relaxation time $\lambda = 0.00011$ for all the simulations.

Numerical testing is first done to find the limiting value of Δt for stability. For $\epsilon = 0.1$, $r = 8\Delta x$, M = 0.5, $\sigma_x \Delta x = \sigma_x \Delta y = 1$ and $D = 20\Delta x$, the results, displayed in Figure 5, confirm that IMEX 3 has a larger stability region than IMEX 2, but for yet unknown reasons IMEX 4 does not have a larger time step than IMEX 3. Stable solutions are obtained for $\Delta t = 0.1\Delta x$ using IMEX2, $\Delta t = 0.9\Delta x$ using IMEX3, and $\Delta t = 0.8\Delta x$ using IMEX4.

The significance of the parameter β , defined in Eq. (23), in the PML formulation is also illustrated in Figure 5. If $\beta = 0$, then the three IMEX schemes are all unstable for values of Δt that were shown to be stable for β as defined in Eq. (23).

Figure 6 shows the density contours at t=10,12 and 16 for $\epsilon = 0.01$, $r = 8\Delta x$, M = 0.25, $\sigma_x \Delta x = \sigma_x \Delta y = 1$ and $D = 10\Delta x$. The absorption of waves inside the PML domain can be observed in the contour plots. Figure 7 confirms the accuracy of the numerical solutions by comparing them to the exact solution at

t=6 and 12. We can see that solutions of all IMEX schemes are in good agreement with the exact solution in the physical domain on the scale of the graph.

To evaluate the reflection error quantitatively, Figure 8 shows the maximum difference between the numerical solution and a reference solution obtained by using a larger computational domain along the line segment defined by the points (45,5) and (45,45). The plotted maximum difference of density is relative to the amplitude of the out-going wave at the exit boundary A_0 (defined as the difference between the peak amplitude at the DVBE and PML interface and the mean flow density) and is plotted as a function of time for different values of PML width D. As the width of the PML layer increases, the reflection error reduces. We can see that a reflection error of less than 0.1% is obtained with a PML width of only 6 grid points with $D = 6\Delta x$.

VII..2. Vorticity Wave

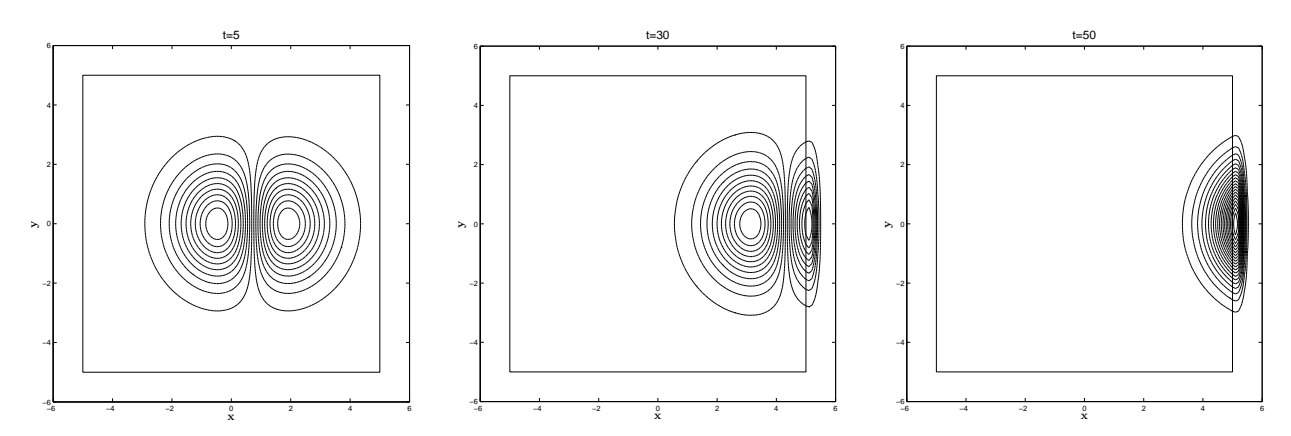


Figure 9. IMEX 3 v-velocity contours for $\epsilon=0.001,\ r=14\Delta x,\ \sigma_x\Delta x=\sigma_y\Delta y=1$ and $D=10\Delta x.$

We also simulate a vorticity wave with the following initial conditions for density ρ and velocity components u and v:

$$\rho = 1$$

$$u = U_0 + \epsilon y \exp\left[-(\ln 2)\frac{x^2 + y^2}{r^2}\right]$$

$$v = V_0 - \epsilon x \exp\left[-(\ln 2)\frac{x^2 + y^2}{r^2}\right]$$

$$U_0 = Mc_s$$

$$V_0 = 0$$
(63)

In Figure 9 we plot the contours of the v-velocity at t=5, 30 and 50 for $\epsilon = 0.001$, $r = 14\Delta x$, $\sigma_x \Delta x = \sigma_y \Delta y = 1$ and $D = 10\Delta x$. We can see from the contour plots that the vorticity wave is effectively absorbed by the PML layer. This is confirmed in Figure 10 as we compare the v-velocity profile to the exact solution at t=5 and 50. The finite difference solution compares well with the exact solution at both times.

To quantify the reflection error, we plot the maximum difference between numerical and reference v-velocity along the line segment defined by the points (45,5) and (45,45) as a function of time for different values of D. For all three IMEX solutions, a reflection error of less than 0.2% is obtained with a PML width $D = 10\Delta x$.

VIII. Conclusions

PML absorbing boundary conditions have been derived for the discreet velocity Boltzmann-BGK equation. Both the split and unsplit formulations are given. Linear analysis of the absorbing equations show that they are stable for numerical simulations. The performance of the absorbing equations as a nonreflecting boundary condition has been assessed by numerical examples using a finite difference method with

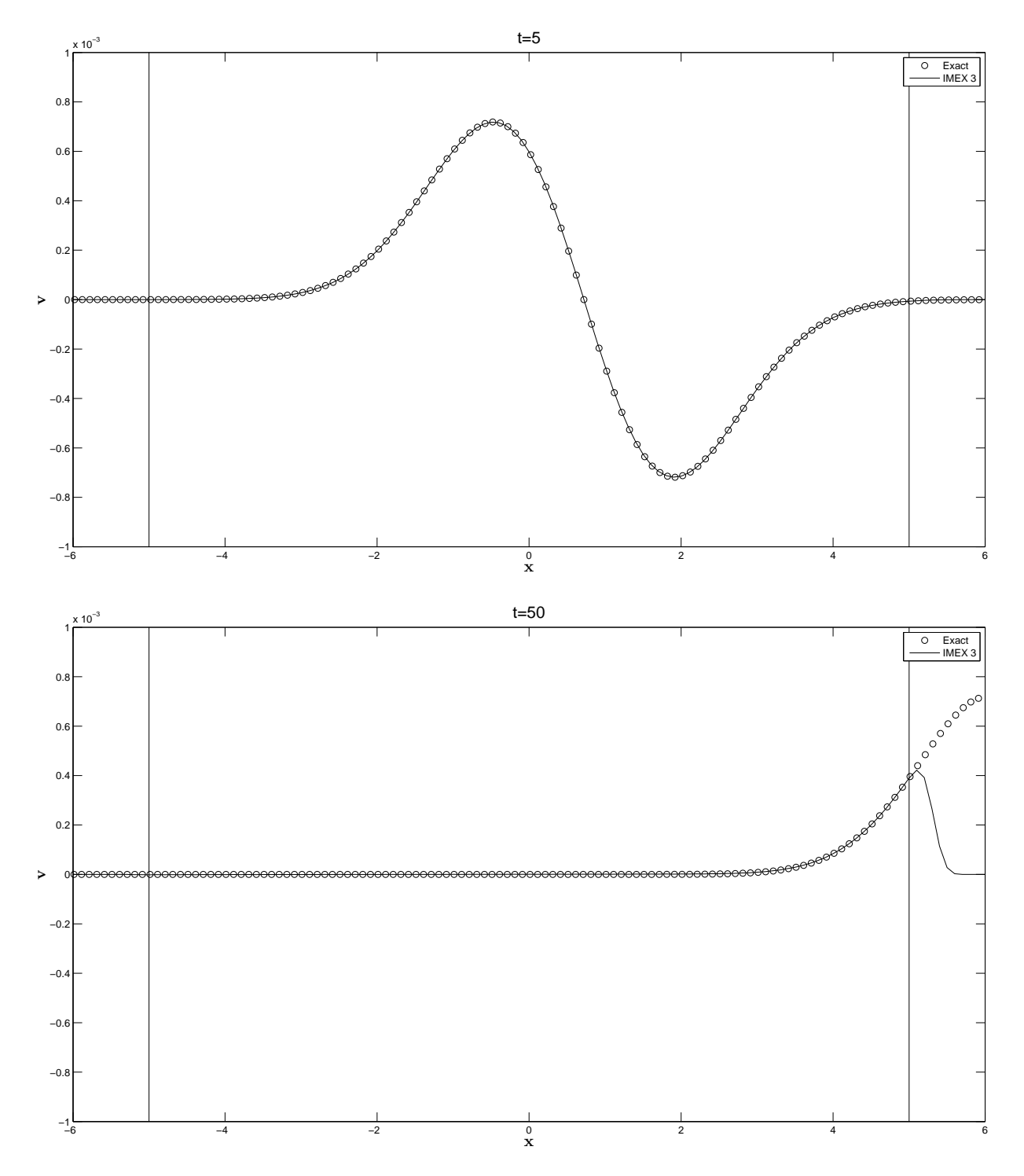


Figure 10. IMEX 3 v- velocity profile for $\epsilon=0.001,\ r=14\Delta x,\ \sigma_x\Delta x=\sigma_y\Delta y=1$ and $D=10\Delta x.$

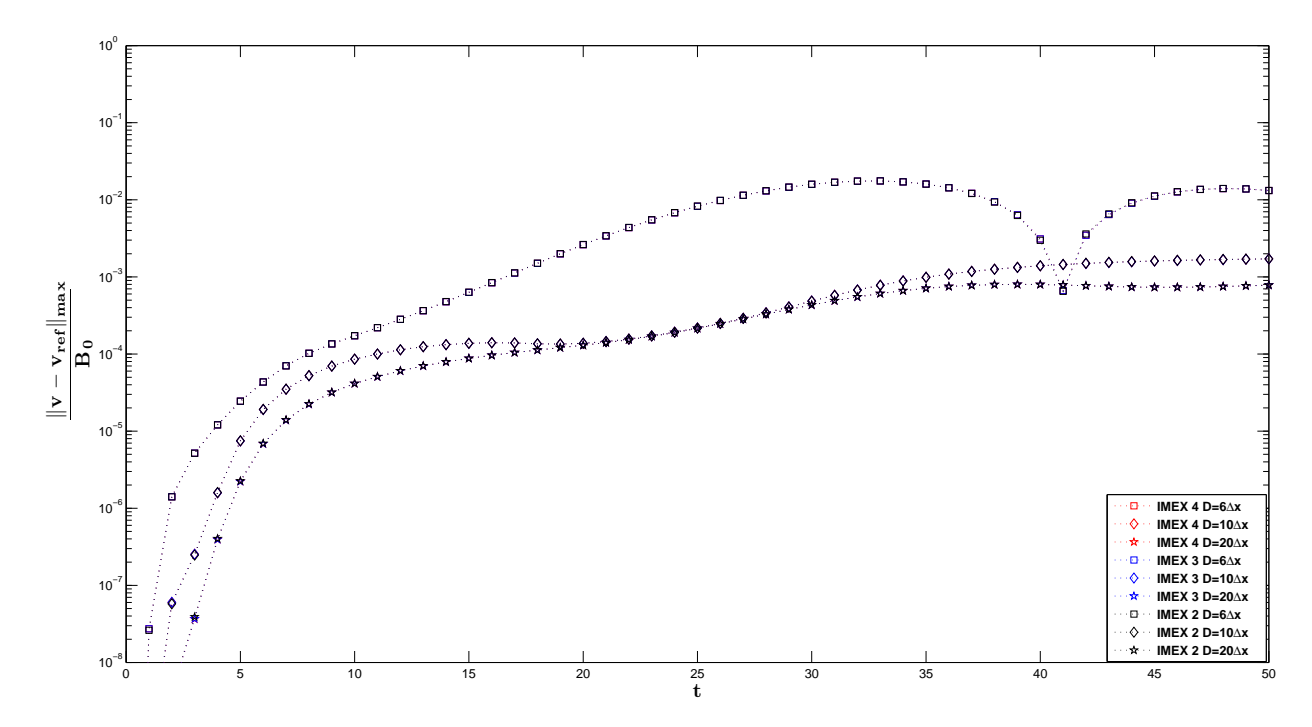


Figure 11. Vorticity reflection coefficient for $\epsilon = 0.001$, $r = 14\Delta x$, M = 0.25, and $\sigma_x \Delta x = \sigma_y \Delta y = 1$. $B_0 = 0.0007$.

implicit-explicit Runke-Kutta schemes. In the examples we considered, the PML equations we proposed performed well. A lattice model for the proposed PML equations will be presented in a future work. The effectiveness of PML equations to absorb outgoing waves that exit the domain is an important step toward using Boltzmann-BGK models to solve aeroacoustic problems.

Acknowledgments

This work is supported by a national Science Foundation (NSF) grant DMS-0810946.

References

¹Huang, K., Statistical Mechanics, Wiley, 1987.

²Bhanatgar, P., Gross, E., and Krook, M., "A Model for Collision Process in Gases. I. Small Amplitude Process in Charged and Neutral One-Component Systems," *Physical Review*, Vol. 94, No. 3, 1954, pp. 511–525.

³Chen, S. and Doolen, G. D., "Lattice Boltzmann Method for Fluid Flows," *Annual Reviews Fluid Mechanics*, Vol. 30, 1998, pp. 329–364.

⁴Shi, Y., Zhao, T. S., and Guo, Z. L., "Finite Difference-Based Lattice Boltzmann Simulation of Natural Convection Heat Transfer in a Horizontal Concentric Annulus," *Computers and Fluids*, Vol. 35, 2006, pp. 1–15.

⁵Stiebler, M., Tolke, J., and Krafczyk, M., "An Upwind Discretization Scheme for the Finite Volume Lattice Boltzmann Method," *Computers and Fluids*, Vol. 35, 2006, pp. 814–819.

⁶Tamura, A. and Tsutahara, M., "Direct Simulation of Acoustic Waves Emitted from Moving Bodies by the Finite Difference Lattice Boltzmann Method," AIAA paper 2006-2489, 2006.

⁷Tsutahara, M., Kataoka, T., Shikata, K., and Takada, N., "New Model and Scheme for Compressible Fluids of the Finite Difference Lattice Boltzmann Method and Direct Simulations of Aerodynamic Sound," *Computers and Fluids*, Vol. 37, 2008, pp. 79–89.

⁸Kam, E. W. S., So, R. M. C., and Leung, R. C. K., "Lattice Boltzmann Method Simulation of Aeroacoustics and Nonreflecting Boundary Conditions," *AIAA Journal*, Vol. 45, No. 7, 2007, pp. 1703–1712.

⁹Najafiyazdi, A. and Mongeau, L., "A Perfectly Matched Layer Formulation for the Lattice Boltzman Method," AIAA paper 2009-3117, 2009.

¹⁰Hu, F. Q., "A Stable, Perfectly Matched Layer for Linearized Euler Equations in Unsplit Physical Variables," *Journal of Computational Physics*, Vol. 173, 2001, pp. 455–480.

¹¹Hu, F. Q., "A Perfectly Matched Layer Absorbing Boundary Condition for Linearized Euler Equations with a Non-Uniform Mean Flow," *Journal of Computational Physics*, Vol. 208, 2005, pp. 469–492.

¹²Pieraccini, S. and Puppo, G., "Implicit-Explicit Schemes for BGK Kinetic Equations," *Journal of Scientific Computing*, Vol. 32, No. 1, 2007, pp. 1–28.

- ¹³Pareschi, L. and Russo, G., "Implicit-Explicit Runge-Kutta Schemes and Application to Hyperbolic Systems with Relaxation," *Journal of Scientific Computing*, Vol. 25, 2005, pp. 129–155.
- ¹⁴Li, Q., He, Y. L., Wang, Y., and Tao, W. Q., "Coupled Double-Distribution-Function Lattice Boltzmann Method for the Compressible Navier-Stokes Equations," *Physical Review E*, Vol. 76, No. 056705, 2007.
- ¹⁵He, X. and Luo, L.-S., "A Priori Derivation of the Lattice Boltzmann Equation," *Physical Review E*, Vol. 55, No. 6, 1997.
- ¹⁶Shan, X., Yuan, X. F., and Chen, H., "Kinetic Theory Representation of Hydrodynamics: A Way Beyond the Navier-Stokes Equation," *Journal of Fluid Mechanics*, Vol. 550, 2006, pp. 413–441.
- ¹⁷Mavriplis, D. J., "Multigrid Solution of the Steady-State Lattice Boltzmann Equation," Computers and Fluids, Vol. 35, 2006, pp. 793–804.
- ¹⁸Marie, S., Ricot, D., and Sagaut, P., "Comparison Between Lattice Boltzmann Method and Navier-Stokes High Order Schemes for Computational Aeroacoustics," *Journal of Computational Physics*, Vol. 228, 2009, pp. 1056–1070.
- ¹⁹Berenger, J. P., "A Perfectty Matched Layer for the Absorption of Electromagnetic Waves," *Journal of Computational Physics*, Vol. 114, 1994, pp. 185–200.
- ²⁰Becache, E., Fauqueux, S., and Joly, P., "Stability of Perfectly Matched Layers, Group Velocities and Anisotropic Waves," Journal of Computational Physics, Vol. 188, 2003, pp. 399–433.
- ²¹Hagstrom, T. and Nazarov, I., "Perfectly Matched Layers and Radiation Boundary Conditions for Shear Flow Calculations," AIAA paper 2003-3298, 2003.
- ²²Hu, F. Q., "On the Construction of PML Absorbing Boundary Condition for the Non-Linear Euler Equations," AIAA paper 2006-0798, 2006.
- ²³Tam, C. K. W. and Webb, J. C., "Dispersion-Relation-Preserving Finite Difference Schemes for Computational Acoustics," *Journal of Computational Physics*, Vol. 107, 1993, pp. 262–281.
- ²⁴Kennedy, C. A. and Carpenter, M. H., "Additive Runge-Kutta Schemes for Convection-Diffusion-Reaction Equations," Applied Numerical Mathematics, Vol. 44, No. 1-2, 2002, pp. 139–181.